

ADVANCES IN LIGHTWEIGHT HEAT SINKS

Mohammad Reza Shaeri*, Richard W. Bonner

Advanced Cooling Technologies, Inc., Lancaster, PA 17601, USA

ABSTRACT

Experiments were performed to investigate the thermal performance of a lightweight heat sink made by perforated folded fins. Perforations with circular cross sections were distributed on the lateral side of fins in a staggered configuration. Results were compared against those of a heat sink without perforations. The results are reported as functions of pumping power, in order to provide a better practical insight about the performance of proposed thermal management solution. It was found that despite slightly increase in the thermal resistance, the perforated-finned heat sink in this study is an appropriate thermal management solution in weight sensitive applications.

KEY WORDS: Lightweight heat sink, Perforated fin, Folded fin, Thermal resistance, Pumping power.

1. INTRODUCTION

In weight sensitive applications like those in aerospace, military, and electric vehicle industries, using lightweight thermal management solutions is essential. Perforated fins as one of the most popular techniques to enhance heat transfer rate in air-cooled heat sinks provide lighter fins as well due to perforations. The logic behind using perforated fins is frequent interrupting the boundary layer and, in turn, enhancing the heat transfer rate [1-5]. In many applications, folded fins are the primary fin design used in air-cooled heat sinks due to their higher fin per inch (FPI) compared with an extruded heat sink, which leads to ultimately higher thermal performances. In the present study, pressure drop and thermal performance of a perforated-finned heat sink (PFHS) made by folded fins, as a lightweight thermal management solution are investigated.

2. EXPERIMENT

The CAD model of the experimental setup and folded fins are illustrated in Fig. 1. A blower provided the airflow through a 2 m long stainless steel duct with a rectangular cross section of 36 cm by 7 cm. The velocities inside the duct were adjusted by regulating voltages of a DC power supply that powered the blower. Two resistance temperature detectors (RTD) probes at the entrance and exit of the heat sink measured the inlet and outlet air temperatures, respectively. The pressure drop across the duct was measured by using a differential pressure transmitter. The top surface of the duct was formed by placing a transparent polycarbonate cover on the duct flange. The duct was airtight by placing an adhesive neoprene rubber gasket between the flange and the cover, which was clamped in place between the cover and the flange. Aluminium fins had the thickness, height, length, flow width, and FPI of 0.25 mm, 19.05 mm, 20.32 cm, 30.48 cm, and 10.5, respectively. An aluminium plate with the thickness of 2.54 mm, and the width and length equal to flow width and length of the fins, respectively, was used as the heat sink base. Seven grooves at different distances from the inlet of the heat sink were machined on the heat sink base to locate seven T-type thermocouples for measuring temperature distributions across the heat sink base. The base plate and folded fins were bonded together using a thermal epoxy. A flexible heater was glued on the heat sink base, and provided a uniform heat load to the base. The heater was powered by a variable transformer, and the electrical power was measured using voltage and current

*Corresponding Author: MohammadReza.Shaeri@1-ACT.com

transducers. To minimize the heat loss to the ambient, the heat sinks were covered by thermal insulation layers. The perforated fins were fabricated from a perforated sheet, made by inserting circular perforations at a diameter, center to center, and porosity of 3.17 mm, 6.35 mm, and 0.22, respectively. The porosity is defined as the ratio of the void area per square inch of the sheet. A solid-finned heat sink (SFHS, a heat sink without perforations) was fabricated and used as the base for comparisons.

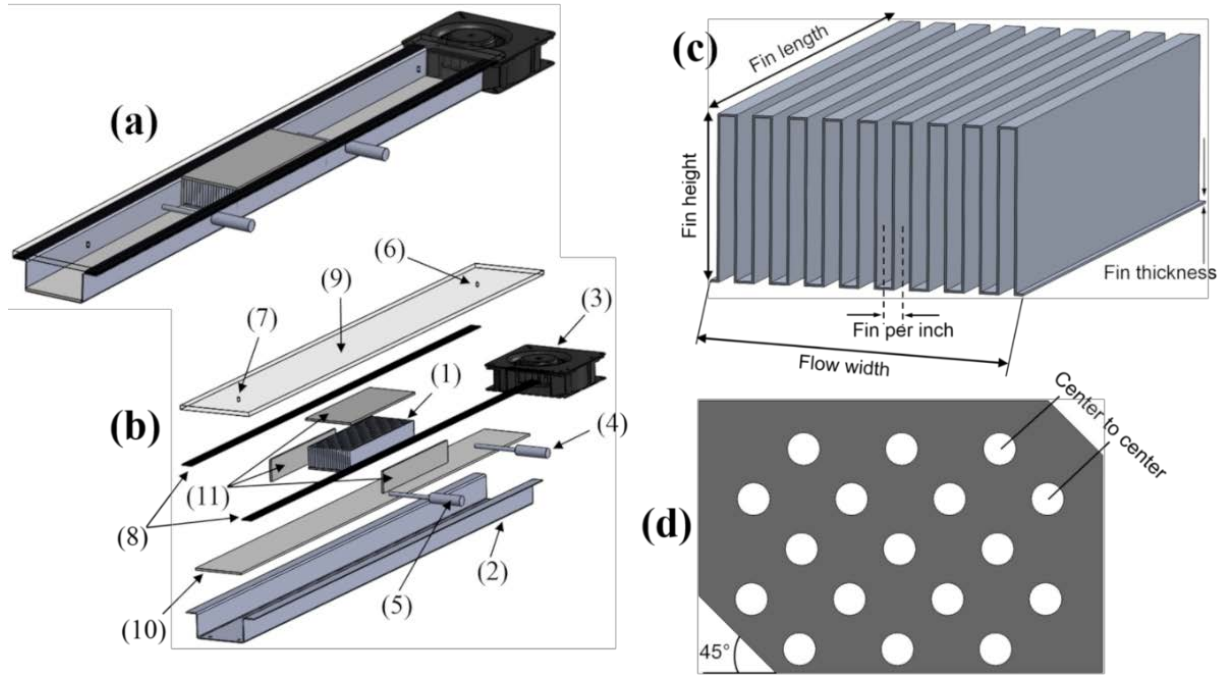


Fig. 1 (a) The CAD model of the experimental setup; (b) 1: heat sink; 2: duct; 3: blower; 4 and 5: inlet and outlet RTD probes, respectively; 6 and 7: high and low-pressure sensors of the differential pressure transducer, respectively; 8: rubber gasket; 9: polycarbonate cover; 10 and 11: insulation layers; (c) the CAD model of the folded fins without perforations; (d) the CAD model of the perforated sheet.

The raw experimental data were collected when the changes in the temperatures obtained by individual thermocouples and RTD probes were below 0.3°C over 10 minutes of operation of the system (steady state condition). The experiments were proceeded by increasing the input blower voltage at a fixed input heat load. The experiments were conducted at different heat inputs. The volume flow rate inside the duct (\dot{V}_d) was determined by using an airflow bench. By measuring the pressure drop across the heat sink (ΔP), the pumping power (P_p) and Reynolds number (Re) are calculated as follows:

$$P_p = \dot{V}_d \times \Delta P \quad (1)$$

$$Re = \frac{D_h}{\nu} \times \frac{\dot{V}_d}{[(FPI \times W) - 1]W_{ch}H} \quad (2)$$

where the term inside the brackets stands for the number of channels. Also W , W_{ch} , and H are the flow width, fin spacing (channel width), and fin height, respectively. In addition, $D_h = 2W_{ch}$, which corresponds the hydraulic diameter of high aspect-ratio fins. By subtracting the sensible absorbed heat by the air from the electrical input heat (Q_{input}), the heat loss from the heat sink to the ambient was negligible (below 5%); therefore, Q_{input} was used for the data reduction.

The thermal performances of the heat sinks are described by the heat sink thermal resistance (R):

$$R = \frac{T_{b,max} - T_i}{Q_{input}} \quad (3)$$

where $T_{b,max}$ and T_i are the maximum temperature on the heat sink base, and the inlet air temperature, respectively. The uncertainties of the instruments were based on the information provided by their manufacturers. Using the uncertainty analysis technique described in [2], the maximum uncertainty of Re , P_p , Q_{input} , and R was below 2.6%, 3.3%, 2.0%, and 2.8%, respectively.

3. RESULTS

Fig. 2 illustrates ΔP across the heat sinks. A higher ΔP in the PFHS is due to flow disturbances inside the channels of a the PFHS because of perforations, as well as the flow interactions over perforations with each other [2-4].

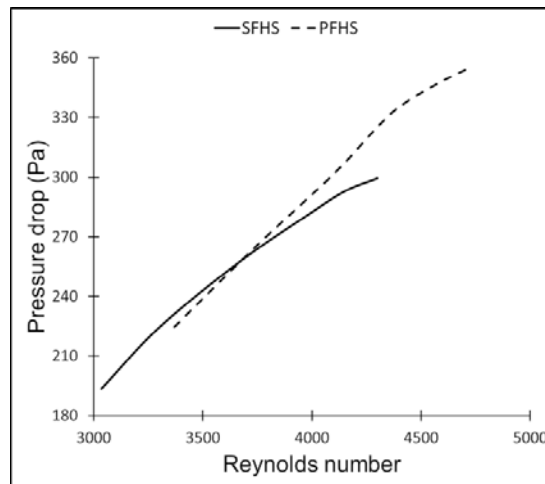


Fig. 2 Pressure drop across the heat sinks that were tested in this study.

To provide a better practical insight, thermal resistances of heat sinks at this study are presented as functions of pumping power as illustrated in Fig. 3.

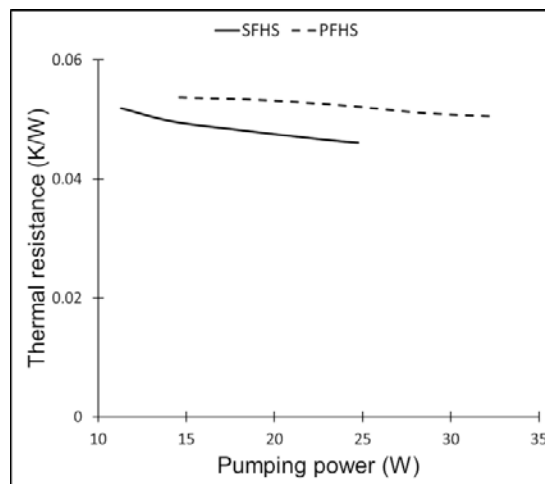


Fig. 3 Thermal resistances of heat sinks at different pumping power.

To have a better comparison between thermal resistances of heat sinks, the percentage of change in the thermal resistance of the SFHS by a PFHS is defined as follows [2-4]:

$$\eta = \frac{R_{PFHS} - R_{SFHS}}{R_{SFHS}} \times 100 \quad (4)$$

where the thermal resistance of each heat sink is identified by its corresponding index. To calculate R_{PFHS} , the raw experimental thermal resistances of the SFHS were correlated to their corresponding pumping powers. Then, this function was used to obtain the equivalent thermal resistance of the SFHS at the pumping power associated with the PFHS [2]. In addition, to assess the thermal benefits of a PFHS as a lightweight thermal management solution, the weight of each heat sink is integrated with its thermal resistance to form a new parameter called mass-based thermal resistance (MBTR) [2-4], as follows:

$$MBTR = M \times R \quad (5)$$

where M is the mass of total fins in the heat sink. The percentage of change in the MBTR of the SFHS by the PFHS is described as follows:

$$\beta = \frac{MBTR_{PFHS} - MBTR_{SFHS}}{MBTR_{SFHS}} \times 100 = \frac{R_{PFHS}(1 - \phi) - R_{SFHS}}{R_{SFHS}} \times 100 \quad (6)$$

where β is calculated using R_{PFHS} and R_{SFHS} that have been already determined for calculating η . Also, ϕ is the porosity. Fig. 4 illustrates η and β as functions of pumping power. This is an interesting figure to select an appropriate heat sink based on the design goal, which can be using a heat sink with either lower thermal resistance or lower weight. Based on Fig. 4, while the PFHS increased the thermal resistance 8.0-13.0%, it reduced the MBTR between 11.9-15.5%. Moreover, the PFHS is almost 22% lighter than the SFHS due to $\phi = 0.22$.

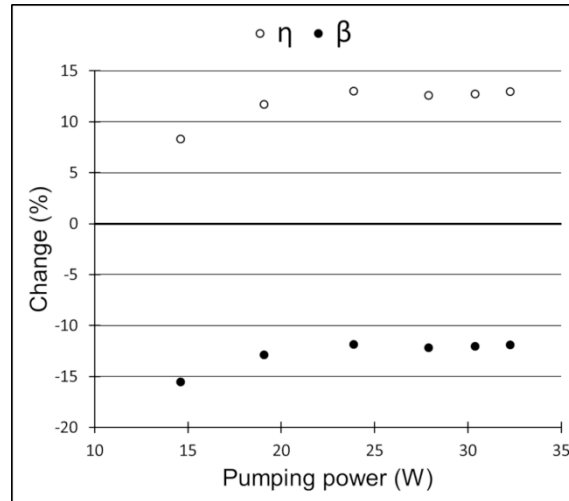


Fig. 4 Percentage of changes in the thermal resistances and MBTR of the SFHS by using the PFHS.

4. CONCLUSIONS

The PFHS resulted in a higher ΔP due to more flow disturbances inside the channels of the heat sink, compared with the SFHS. Despite slightly increase in the thermal resistances by using the PFHS, this heat sink reduced the MBTR up to 15.5%. In addition, the PFHS is almost 22% lighter than the SFHS. Therefore, reduction in both MBTR and weight, despite a slight increase in thermal resistance, signifies that the proposed PFHS in this study is a promising thermal management solution in weight sensitive applications.

ACKNOWLEDGMENT

Support by the Office of Science in the U.S. Department of Energy, award# DE-SC0011317 is acknowledged.

REFERENCES

- [1] Yaghoubi, M., Shaeri, M.R., Jafarpur, K., "Three-dimensional numerical laminar convection heat transfer around lateral perforated fins," *Computational Thermal Sciences*, 1, pp. 323-340, (2009).
- [2] Shaeri, M.R., Bonner, R., "Laminar forced convection heat transfer from laterally perforated-finned heat sinks," *Applied Thermal Engineering*, 116, pp. 406-418, (2017).
- [3] Shaeri, M.R., Bonner, R., "Heat transfer and pressure drop in laterally perforated-finned heat sinks across different flow regimes," *International Communications in Heat and Mass Transfer*, 87, pp. 220-227, (2017).
- [4] Shaeri, M.R., Bonner, R.W., "Lightweight and High-Performance Air-Cooled Heat Sinks," 34th Thermal Measurement, Modeling & Management Symposium (SEMI-THERM), IEEE, pp. 224-227, (2018).
- [5] Ismail, M.F., Hasan, M.N., Saha, S.C., "Numerical study of turbulent fluid flow and heat transfer in lateral perforated extended surfaces," *Energy*, 64, pp. 632-639, (2014).